J Mar Sci Technol (2004) 9:1–13
DOI 10.1007/s00773-003-0164-4

Journal of
Marine Science
and Technology

Original articles

Wave impact underneath horizontal decks

Rolf Baarholm[1] and Odd M. Faltinsen[2]

[1] Norwegian Marine Technology Research Institute (MARINTEK), PO Box 4125 Valentinlyst, N-7450 Trondheim, Norway
[2] Department of Marine Technology, NTNU, N-7491 Trondheim, Norway

Abstract The problem of water impact on a fixed horizontal platform deck from regular incident waves was studied. Two-dimensional potential flow was assumed, and the resulting boundary-value problem was solved by three alternative numerical methods, a method based on a generalization of the impact theory by Wagner, and two different nonlinear boundary-element methods. The Wagner-based method used a von Karman approach during the water exit phase, i.e., when the wetted surface decreases. Experiments of the impact on an idealized platform deck have been performed to validate the theory. Comparisons show that the Wagner-based method yields good results for the water entry phase, when the wetted deck area increases, but poor results when the wetted area diminishes. The boundary-element methods compare well with experiments for the entire impact process. A Kutta condition is necessary at the aft body–free surface intersection during water exit and when the flow separates from the aft edge. Gravity effects matter for the water exit phase.

Key words Hydrodynamics · Water impact · Boundary element methods

Introduction

Water impact loads on offshore structures have been of concern to designers for the past 25 years. In the early years, the main interest was focused on impact forces on horizontal structural members located in the splash zone, see e.g., Dalton and Nash,[1] Faltinsen et al.,[2] and Sarpkaya.[3] Water impact on the decks of platforms was of less concern.

It is common practice to design the lower deck of offshore platforms to be above the maximum predicted wave level. Knowledge regarding wave heights and the variability of environmental conditions with time was limited at the time when the first-generation bottom-mounted oil-platforms were designed, and even if a platform is designed with a safe deck clearance initially, this might be reduced over time. This reduction can be caused either by settlement of the platform due to its own weight, or by foundation subsidence and reservoir compaction. Therefore, the deck may be subjected to wave-induced loads that were not accounted for in the original design. Owing to these uncertainties in the safety level, it is important to obtain an accurate prediction of the hydrodynamic loads on the structure induced by wave impact underneath the decks of existing fixed platforms. The significant level of subsidence at the Ekofisk field revealed the need to reexamine all the platforms in the area with respect to wave impact.[4]

When oil and gas production moves to deeper waters, bottom-mounted platforms become less applicable. In deep waters, floaters such as semisubmersibles are often used. For floaters, it has generally been customary to neglect any probability of waves reaching the deck by relying on the deck height to provide a sufficient margin of safety. The deck height of floaters is limited by weight and stability considerations, and this makes the air-gap a substantial cost drives for the platform. In the design of new floaters, one might allow some extreme waves to hit the deck structure. A reduction of the deck's clearance to the still-water level of existing floaters may occur involuntarily when they are in a damaged condition or after a failure in their ballast systems. The deck clearance of existing platforms may also be decreased if higher production volumes are desired. Accordingly, increased storage capacity and deck weight must be compensated for by increased draft, and thus a smaller deck clearance. This implies a higher risk of wave impacts.

Water impacts underneath the decks of platforms may roughly be categorized into global and local impacts. The former occur when a massive wave reaches

Address correspondence to: R. Baarholm
(Rolf.Baarholm@matintek.sintef.no)
Received: February 24, 2003 / Accepted: September 1, 2003

the deck at one end and propagates along the deck. This induces large loads on the deck, and it can be critical for the global strength and overall stability of the platform. In this case, a good structural deck design requires an accurate assessment of both the wave kinematics and hydrodynamic load responses due to wave impact. An approximate solution for impact on a fixed horizontal deck, based on Wagner's solution,[5] was presented by Baarholm and Faltinsen,[6] while Baarholm et al.[7] extend the approach to account for platform motion. Linear wave-induced motion was generated from predescribed transfer functions, while the water-impact-induced response was solved and added to the linear motion to get an estimate of the total platform response. The water impact had a clear influence on the platform motion. A boundary-element method for the perturbation velocity potential due to impact was presented by Baarholm and Faltinsen[8] and Baarholm.[9] Comparisons with experiments show that this method yields a significant improvement compared with the Wagner-based method. Nevertheless, the method has flaws, which prompted the further developments presented here.

In addition to massive impact events, run-up of water along platform legs may also cause water impacts underneath the platform deck, and local wave amplification due to wave diffraction from vertical platform members can also cause water impact on the deck. These impacts are localized in space, and are crucial to local structural responses and to the comfort of the platform crew, but they are less important in terms of global effects.

The main topic of this article is the global loads on a fixed horizontal deck due to the impact of a massive wave. A synopsis of our previously published work on the subject of wave-in-deck events, as well as the latest developments are presented. Experiments on impacts on an idealized horizontal deck have been performed. A brief description of these experiments and some observations are given. Furthermore, three theoretical approaches are used to solve the wave-in-deck problem. The first is a simplified Wagner-based method, while the other two are boundary-element methods solving the perturbation velocity potential due to the impact and the total velocity potential, respectively. All three methods have been used to reproduce the experiments, and comparisons of numerical and experimental results are presented. Local impact events are not considered in this work.

Experiments and physical observations

Experiments were performed to validate the theory and numerical solution used to solve the wave-impact problem. Since the numerical modeling is based on physical observations in the laboratory, the experimental part of the work will be described before the theory and the solution procedure.

The experiments were carried out in the flume at the Department of Marine Hydrodynamics, NTNU. This is a narrow wave flume, which is 13.5 m long, 1.3 m deep, and 0.6 m wide. It is designed for a water depth of 1.0 m. The flume walls are made of glass, which provides good visual observations. An electronically operated, computer-controlled, single-flap wave-maker is installed in the flume. The wave-maker is fitted with a control system that allows the flap to damp out reflected waves. The flap is hinged 0.10 m above the bottom of the flume. At the downstream end of the flume, a parabolic beach is installed. These facilities allow for near 2-D experiments to be performed. A box-shaped deck model with no obstructions underneath was used in the experiments. The deck covered the entire width of the tank, and was stiff enough for hydroelastic effects to be insignificant. Moreover, the model was fitted with 0.30 m high side walls to keep water from flowing into the model from above. The vertical load on the deck was the primary parameter to be measured, but the wetted area underneath the deck and the free-surface elevation at different positions were also measured. The bottom plate was 0.63 m long and 0.56 m wide, and the clearance between the deck and the mean free surface could easily be changed. The model was placed in the middle of the flume, equally far from the wave-maker and the beach. Figure 1 shows a sketch of the model and the primary instrumentation used. A more detailed description of the experimental set-up is given elsewhere.[9]

Regular waves were used in the experiments, and the model was kept out of reach of the waves until a steady state was reached. The deck was then lowered to the desired deck height. Figure 2 shows sketches of the impact process as a wave hits the deck. The sketches are based on observations in the flume. As the wave hits the front end of the deck, the wetted length increases smoothly, and a pile-up of water and a thin jet are formed on the upstream side of the model. Compared with the undisturbed wave, a considerable pile-up of water downstream of the wetted body caused by the impact will be present. The profile of the free surface at a small distance downstream of the wetted part of the body is smooth, with moderate curvature. In Fig. 2c, the upstream body/free surface intersection has just moved around the front corner to the bottom plate of the deck. The free surface near the intersection is characterized by high curvature. As the flow reaches the aft end of the deck, the fluid flow leaves the deck tangentially. This implies that a fluid particle on the free surface at the intersection has no vertical velocity. Spray and wave breaking behind the body dissipate energy from the system. After some time, the downstream intersection

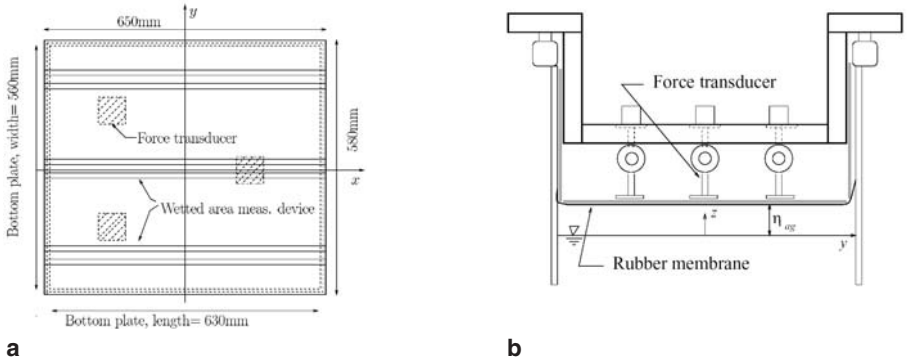

Fig. 1. The model used in the experimental work. **a** Fish-eye view and **b** front view

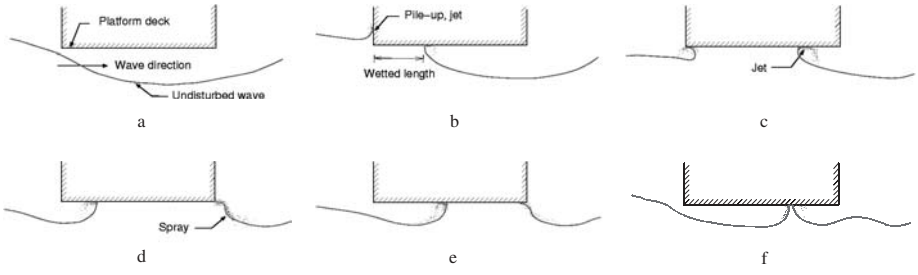

Fig. 2. Behaviour of the physical flow during the first wave impact on the deck

starts to move forward again, and finally the water detaches from the deck in the manner shown in the last sketch. The duration of the water exit phase is longer than that of the water entry phase. The time-history for the vertical force on the deck is characterized by a positive upward-directed force peak during water entry, followed by a negative force peak during water exit. The magnitude of the negative force peak is usually larger than the corresponding positive one.

A difference in the impact process when the first wave hits the structure and impacts due to the following waves was noted. The disturbance of the free surface caused by the preceding impact process causes a double slam event where the second impact occurs in the vicinity of the final detachment of the preceding wave. This gives a significant positive force peak of short duration. This phenomenon has not been studied numerically, but the physics was discussed previously.[9]

Theory and solution procedure

In the theoretical description of the wave-in-deck problem, an incompressible fluid in two-dimensional, irrotational flow is assumed. Accordingly, potential flow is applied and viscous effects are disregarded. For a real platform, the approximation of two-dimensional flow requires head or beam sea, and that the incident waves are long relative to the diameter of the platform legs. Further, the wetted length must be much smaller than the wetted breadth. Moreover, the effects of hydroelasticity and surface tension are disregarded. A boundary value problem for the total velocity potential Φ can be set up. The two-dimensional Laplace equation becomes the governing equation in the fluid domain:

$$\nabla^2\Phi = \frac{\partial^2\Phi}{\partial x^2} + \frac{\partial^2\Phi}{\partial z^2} = 0 \tag{1}$$

The (x, z)-coordinate system has its origin in the mean free surface with the z-axis pointing upwards. Boundary conditions are required to solve the problem. In particular, by setting the pressure equal to the atmospheric pressure on the free surface, S_F, a dynamic free surface condition in the form

$$\frac{\partial\Phi}{\partial t} + \frac{1}{2}\left[\left(\frac{\partial\Phi}{\partial x}\right)^2 + \left(\frac{\partial\Phi}{\partial z}\right)^2\right] + g\zeta = 0 \qquad \text{on } S_F \tag{2}$$

follows from Bernoulli's equation. S_F is described by $z = \zeta(x, t)$, where ζ is the free-surface elevation. A kinematic free-surface condition must also be imposed. This condition states that fluid particles on the free surface remain on the free surface, and it can be written as

$$\frac{\partial\Phi}{\partial z} = \frac{\partial\zeta}{\partial t} + \frac{\partial\zeta}{\partial x}\frac{\partial\Phi}{\partial x} \qquad \text{on } z = \zeta(x,t) \tag{3}$$

Another way of satisfying the kinematic free-surface condition is to follow the track of free surface particles.

This procedure was used in this study. Furthermore, the boundary condition

$$\frac{\partial \Phi}{\partial n} = U_n \qquad \text{on } S_B \tag{4}$$

which requires the body to be impermeable, must be satisfied on the instantaneous wetted body surface, S_B. In Eq. 4, U_n is the body's velocity normal to its own surface, and thus for a fixed body, as studied here, $U_n \equiv 0$, where $\partial/\partial n$ denotes the derivative along the normal unit vector $\boldsymbol{n}$, and $\boldsymbol{n}$ is defined as being positive when pointing into the fluid domain. For finite water depths, a similar condition must be imposed on the bottom, but in this work the water depth was assumed to be sufficiently large relative to the wavelength for the bottom condition to be omitted, since addition initial conditions would be needed.

Three alternative theoretical approaches have been used to study this problem: a Wagner-based method, and two different approaches applying Greens' second identity. The former solves the perturbation velocity potential due to the impact, and the latter solves the total velocity potential.

Wagner-based method

The exact 2-D boundary value problem for the wave-in-deck event is given above. In what follows, a few additional assumptions will be made, and a method based on the impact theory by Wagner[5] will be established. The total velocity potential is now written as $\Phi = \phi + \phi_I$, where ϕ and ϕ_I are the perturbation potential due to the impact and the velocity potential of the undisturbed incident waves, respectively. The latter is assumed to be known a priori, and the boundary-value problem (BVP) for ϕ is set up. Second-order regular incident waves are assumed. The Laplace Eq. 1 becomes the governing equation in the fluid domain. The effect of gravity is neglected, and the high-frequency dynamic free-surface condition, $\phi = 0$, is applied on the horizontal line $z = 0$. The local (x, z)-coordinate system has its origin in the center of the instantaneous wetted length of the deck, with the positive x-axis in the direction of the waves, and with the z-axis pointing upward. This free-surface condition implies that no waves will be generated. Futhermore, the body boundary condition is approximated as $\partial\phi/\partial z = -V_0 - V_1 x$, and it is imposed at $|x| \le c(t)$ and $z = 0$, where $c(t)$ is the half-breadth of the wetted length. The resulting BVP can be solved analytically for each time-step. This yields

$$\phi = -V_0\sqrt{c^2 - x^2} - \frac{1}{2}V_1 x\sqrt{c^2 - x^2} \qquad \text{on } z = 0 \text{ and } |x| \le c \tag{5}$$

for the perturbation velocity potential on the body, and

$$\frac{\partial \phi}{\partial z} = \frac{V_0|x|}{\sqrt{c^2 - x^2}} + \frac{1}{2}\operatorname{sgn}(x)V_1\left(\sqrt{c^2 - x^2} - \frac{x^2}{\sqrt{c^2 - x^2}}\right) - V_0 - V_1 x \qquad \text{on } z = 0 \text{ and } |x| > c \tag{6}$$

for the impact-induced vertical velocity on the free surface. The evolution of $c(t)$, which determines the wetted length, is unknown, and must be solved numerically. Water hits the front end first, and during the initial increase in wetted length underneath the deck the aft body/free surface intersection point propagates downstream, while the upstream intersection is fixed at the front end of the deck. The free surface on the downstream side is discretized by fluid particles that are tracked in time. Let superscripts j and i denote the time instant and the fluid particle, respectively, so that P_i^j is the position of particle i at $t = t^j$ (Fig. 3). The horizontal velocity of particle i is disregarded, and the new intersection point c^{j+1} is determined a priori, while the time-increment $\Delta t^j = t^{j+1} - t^j$ is found from a local analysis of the time that particle i needs to cover the vertical distance Δz. The time-increment can be written as $\Delta t^j = (\mathrm{d}t/\mathrm{d}c)_m(c_i^{j+1} - c_{i-1}^j)$, where $(\mathrm{d}t/\mathrm{d}c)_m$ is found by matching a local "corner flow" velocity potential valid in the vicinity of the intersection point with Eq. 5, and averaging over the time-increment. The local solution is introduced because of the singular nature of the fluid velocity at the intersection points. The details of this procedure are given elsewhere.[9] Once the time-increment is determined, the free surface particles are moved with their local velocities due to both ϕ and ϕ_I, and the new free-surface position ζ^{j+1} is found. A fourth-order Runge–Kutta scheme is used for the time integration. Velocities due to ϕ_I above the mean free surface are found by a Taylor expansion consistent to second order. Once the downstream intersection point has reached the aft end of the deck, it is kept fixed there during the water exit phase. In this phase, the upstream intersection point is determined by a von Karman-type

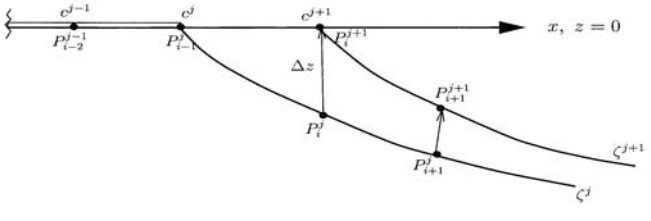

Fig. 3. Stepping of the free surface in the Wagner-based method. The figure shows a close-up of the body and the free surface near the downstream intersection point. c^j and c^{j+1} are the chord length at time instants t^j and t^{j+1}, respectively

approach, i.e., as the intersection between the deck and the incident wave. A Wagner method will not give a solution during the water exit phase. The vertical force on the deck can be found from direct integration of the pressure $-\rho(\partial\phi/\partial t + \partial\phi_I/\partial t + gz)$, where $z = 0$ now refers to the mean free surface, or from the formula

$$F_3 = \frac{\mathrm{d}}{\mathrm{d}t}\left(A_{33}^{(\infty)}V_0\right) + F_{3I} = \rho\pi c\dot{c}BV_0 + \frac{1}{2}\rho\pi c^2 B\dot{V}_0 + F_{3I} \quad (7)$$

where $A_{33}^{(\infty)} = 0.5\rho\pi c^2 B$ is the high-frequency added mass of the wetted deck area, F_{3I} is the nonlinear Froude–Kriloff and hydrostatic force, and B is the wetted breadth. The term proportional to V_0 is denoted as the slamming force, and is governed by the rate of change of the wetted area, while the second term is an added mass force. In accordance with Kaplan,[10] the slamming term is set equal to zero during water exit. This method converges nicely when the density of fluid particles is increased.[9]

Boundary-element method for the perturbation velocity potential

A common method for solving nonlinear free-surface problems is to use Green's second identity to establish an integral equation for the velocity potential.[11] When incident waves are present, two alternative approaches may be applied. One may solve the boundary value problem for the total velocity potential, or one may split the problem as $\Phi = \phi + \phi_I$ and solve for the impact potential. Both approaches are presented, starting with the latter.

As in the Wagner-based method, the incident wave velocity potential and elevation are described a priori by second-order theory, and the perturbation velocity potential ϕ due to the presence of the body is solved. The coordinate system used below has its origin in the mean free surface with the vertical axis pointing upward through the center line of the body. The incident waves propagate in the direction of the positive x-axis. The perturbation velocity potential due to wave impact, ϕ, is unknown and has to be determined. The exact dynamic free-surface condition can be written according to a Lagrangian description as

$$\frac{D\Phi}{Dt} = \frac{1}{2}\left|\nabla\Phi\right|^2 - g\zeta \qquad \text{on } z = \zeta(x,t) \quad (8)$$

Now, assuming that $\Phi = \phi + \phi_I$ and $\zeta = \zeta_D + \zeta_I$, where ζ_D is the surface elevation associated with the disturbance, a dynamic free-surface condition for ϕ can be expressed as

$$\frac{D\phi}{Dt} = \frac{1}{2}\left|\nabla\phi\right|^2 + \nabla\phi\cdot\nabla\phi_I - g\zeta_D \qquad \text{on } z = \zeta(x,t) \quad (9)$$

Terms involving ϕ_I are found by using a Taylor expansion correct to the order $O((k\zeta_a)^2)$, where ζ_a is the amplitude of the first-order incident wave.

In the Wagner based-method, only the wetted part of the bottom plate was taken into account in the boundary-value problem. This means that the wetting of the vertical sides of the deck was neglected. Further, the spatial variation in the impact velocity was approximated by a linear function. Here, the exact body boundary condition according to Stokes' second-order theory is utilized, i.e.,

$$\frac{\partial\phi}{\partial n} = -\frac{\partial\phi_I}{\partial n} \qquad \text{on } S_B \quad (10)$$

where S_B is the instantaneous wetted part of the body. As for the free-surface condition, a Taylor expansion correct to second-order about $z = 0$ is used to find the undisturbed velocities on the body.

As is customary in the mixed Eulerian–Lagrangian method for free-surface flows, the problem is divided into two steps, which are solved in sequence. These steps are described elsewhere.[11] In the first step, the kinetic problem for the perturbation velocity potential is solved with the specified mixed Dirichlet–Neumann boundary conditions. In the second step, the free-surface conditions are integrated in time to update the geometry and the value of the perturbation velocity potential on the free surface.

The kinetic problem for ϕ is solved through Green's second identity. Inside the fluid domain, the velocity potential can be represented in terms of boundary integrals through Green's second identity as

$$-2\pi\phi(x,z,t) = \oint_S \left(\phi(\xi,\eta)\frac{\partial\log r}{\partial n(\xi,\eta)} - \frac{\partial\phi(\xi,\eta)}{\partial n(\xi,\eta)}\log r\right)\mathrm{d}S(\xi,\eta) \quad (11)$$

Here, $r = \sqrt{(x-\xi)^2 + (z-\eta)^2}$, (x, z) is the field point where ϕ has to be evaluated, and (ξ, η) are integration variables. S is a surface enclosing the fluid domain, which comprises the instantaneous free surface S_F and body surface S_B, and vertical control surfaces infinitely far away from the body S_∞. The problem is solved in time as a transient initial value problem, with initial condition $\phi = 0$ on $z = \zeta_I$. S_∞ is taken so far away from the body that its contribution to the integral Eq. 11 is zero. Far away from the body, the free-surface condition becomes $\phi = 0$ on $z = \zeta_I$. For $|x| > x_b$, denoted as the far field region, approximations are imposed. The free-surface condition $\phi = 0$ is taken on $z = 0$. The magnitude of x_b is large compared with the wetted deck length. In the far field region, the flow is almost unaffected by the details

of the body, and ϕ may be expressed as the sum of a vertical dipole and a multipole at the origin, i.e.,

$$\phi = \frac{A_1 z}{x^2 + z^2} + \frac{A_2 xz}{\left(x^2 + z^2\right)^2} \tag{12}$$

The first and second terms account for dominating symmetric and antisymmetric disturbances, respectively. It is now possible to integrate the contribution of far field regions to the integral in Eq. 11 from S_F analytically. A_1 and A_2 are unknown dipole and multipole strengths, respectively.

In the numerical solution, an integral equation based on Eq. 11 is set up by letting (x, z) approach points on S for each time-step. The free surface inside $-x_b < x < x_b$ and the instantaneous wetted body S_B, are divided into N straight line elements, where ϕ and $\partial\phi/\partial n$ are set to be constant over each segment, ϕ is unknown on S_B and known on S_F, and $\partial\phi/\partial n$ is unknown on S_F and known on S_B. Equation 11 is satisfied at the midpoint of each element. This yields a set of N linear equations. However, when the dipole and multipole strengths, $A_1(t)$ and $A_2(t)$, are included, the total number of unknowns is $N + 2$. Two additional equations are obtained by requiring continuity in the velocity potential at $x = -x_b$ and $x = x_b$, and a system of linear equations with the same number of equations as unknowns is obtained. The linear equations are solved by a standard procedure. The equation system is modified, as described later, when the Kutta condition is imposed.

The kinematic problem involves updating the velocity potential on S_F with time, and updating the instantaneous position of the free surface. This is done by time-integration of the corresponding dynamic and kinematic free-surface conditions. Special care is necessary in describing the motion of the free surface, and a time-integration procedure similar to the one described by Zhao and Faltinsen[12] is implemented. This method ensures good conservation of fluid mass.

A precise evaluation of the wetted part of the body is crucial for a correct determination of the load on the body. This can be separated into two separate tasks: determining the upstream and downstream body/free-surface intersection points. Evaluation of the upstream intersection point is most problematic in the short phase, when the intersection point moves around the corner from the front side of the deck to the underside of the deck. The numerical scheme is based on careful inspections of pictures and video recordings of this transition. As the fluid flow goes around the front corner of the deck, the upstream intersection, I_{up}, is held fixed at the corner until $\alpha > \alpha_F$, where α is the angle between the x-axis and the free-surface element next to the body on the upstream side (Fig. 4). I_{up} is then set to propagate freely downstream. The value of α_F has to be chosen

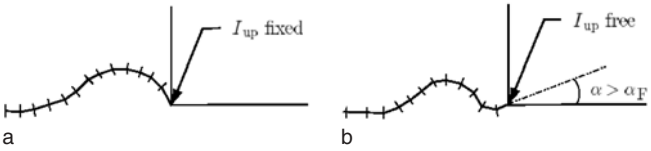

Fig. 4. The numerical procedure for moving the upstream body/free-surface intersection point around the front corner of the deck. **a** The intersection point is kept fixed. **b** $\alpha > \alpha_F$ and I_{up} can move freely

properly. If α_F is too small, I_{up} tends to move too quickly when let free, and as a consequence the solution may break down. $\alpha_F = \pi/10$ seems to yield stable solutions. For the phase where is I_{up} kept fixed, numerical instabilities/errors occur, but when it is set free to move, then stability is regained. If small free-surface elements are used locally, the transition phase has a short duration in the numerical solution, and the global force is not sensitive to the choice of α_F. However, if details of the pressure distribution around the front edge are studied, a more accurate local method is needed. A more thorough discussion of the choice of α_F is given elsewhere.[9] The very high curvature of the free surface as a consequence of the free surface turning around the front edge (see Fig. 1c) also occurred in a similar situation in the numerical studies by Faltinsen et al.[13] of bottom-slamming on a very large floating structure (VLFS) with a shallow draft. Then, a nonlinear boundary-element method (BEM) was also used, but it was not necessary to use the artificial procedure described previously.

The downstream body/free-surface intersection point is denoted I_{dwn}. During the water entry phase, i.e., when I_{dwn} propagates downstream along the bottom plate of the deck, I_{dwn} is found by extrapolation of the free surface onto the body. This yields a time-history for the wetted area that compares well with both experiments and with the Wagner-based method. When I_{dwn} reaches the aft end corner of the deck, the fluid flow leaves the deck tangentially. This can also be noted from the snapshot in Fig. 5a. The pictures show a close-up of the aft end of the body and of the local free surface. The white line indicates the free surface, and its intersection with the body is located at the aft corner of the deck. As long as the aft end of the underside of the horizontal deck is wetted, the free surface at I_{dwn} is horizontal. In the numerical solution, this can be obtained by imposing a condition that requires ϕ to be continuous and the flow to be horizontal at I_{dwn}. This condition will henceforth be denoted the Kutta condition. The integral Eq. 11 is satisfied on the N element midpoints. However, since an additional condition stating a continuous ϕ at I_{dwn} is formulated, the integral equation cannot be satisfied at more than $N - 1$ midpoints. Therefore, it was decided to replace the body boundary condition at midpoint

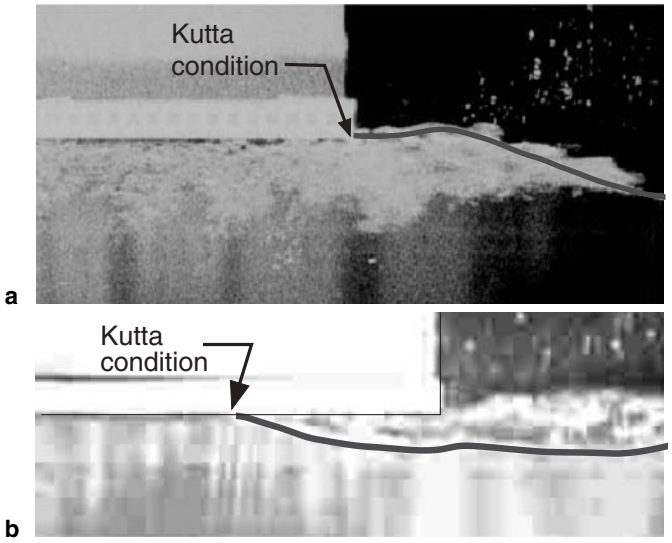

Fig. 5. The fluid flow at the aft body–free-surface intersection point. The flow leaves the deck almost tangentially. **a** Kutta condition at aft and. **b** Kutta condition during the stage of final water exit

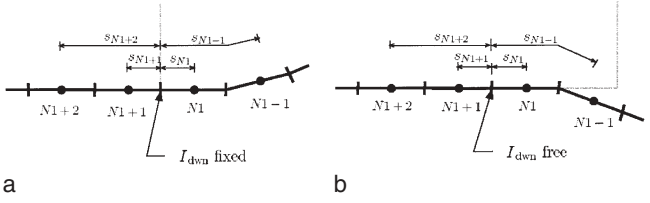

Fig. 6. Close-up of the body and the free surface close to I_{dwn}. The *solid circles* symbolize element midpoints where Eq. 11 is satisfied. s_i is the curvilinear distance from I_{dwn} to midpoint i. **a** Kutta condition at the aft end corner. **b** Kutta condition when I_{dwn} moves upstream

$N1 + 1$ (Fig. 6) with the Kutta condition. The Kutta condition is written as

$$\left(1-\frac{s_{N1+1}}{s_{N+2}-s_{N1-1}}\right)\phi_{N1+1}+\frac{s_{N1+2}}{s_{N1+2}-s_{N1-1}}\phi_{N1+1} =\left(1-\frac{s_{N1}}{s_{N+2}-s_{N1-1}}\right)\phi_{N1}+\frac{s_{N1-1}}{s_{N1+2}-s_{N1-1}}\phi_{N1-1} \quad (13)$$

where ϕ_i is the perturbation velocity potential at midpoint i, and s_i is a curvilinear distance along the body and the free surface, so that s_i is the distance from I_{dwn} to midpoint i. Note that ϕ_{N1+1} and ϕ_{N1+2} are unknowns, while ϕ_{N1} and ϕ_{N1-1} are known quantities. Moreover, continuity is required in the slope of the body and the free surface at the intersection point. This procedure is analogous to the one used by Faltinsen and Pettersen[14] at the separation point for flow around blunt bodies. When the fluid reaches the aft end of the deck, a new horizontal free-surface element is introduced at the intersection. This element is small initially, but is allowed to grow with the speed of the local horizontal velocity of the fluid flow until it is the same size as the neighboring free-surface element. Thereafter, the element size is kept fixed. The dynamic free surface condition is used to step the value of ϕ_{N1}.

In the final stage of water exit, I_{dwn} will start to propagate upstream until the water separates from the deck, as shown in Fig. 2e. Video recordings show that the free surface in the vicinity of I_{dwn} is almost horizontal in this case also. Therefore, the Kutta condition is used in this phase. I_{dwn} is allowed to propagate upstream when the slope of element number $N1 - 1$ and the total vertical velocity of the corresponding midpoint are both negative. The velocity of the intersection point is set to be

$$U_{I_{\mathrm{dwn}}}=\frac{\partial\Phi}{\partial x}=\frac{\partial\phi}{\partial x}+\frac{\partial\phi_{\mathrm{I}}}{\partial x} \quad (14)$$

This provides a stable solution that makes it possible to simulate water exit until the deck becomes almost entirely dry. Numerical instability may occur near the end of the water exit process. This may be caused by elements on the body which are too small compared with the nearby free-surface elements. Consequently, the simulations are stopped before the deck is entirely dry. However, in this phase, the force on the deck is small.

The reason why we have used the Kutta condition is directly related to experimental flow observations. One could say that the same is true about why the Kutta condition is used for a lifting foil. This should also suggest that the use of the Kutta condition is in some way connected with the condition that the "angle of attack" of the incident flow has to be small. This means that the ambient horizontal velocity has to be large relative to the vertical velocity. Further experimental studies are needed to clarify this dependence. It should be noted that the use of a Kutta condition in our case does not mean that vortices are introduced, as is done to describe the flow around a lifting foil.

The main purpose of these calculations was to determine the force of the waves and the resulting force acting on the platform deck. The total force on the body may be computed by using two alternative approaches, direct pressure integration or conservation of fluid momentum. The total pressure on the body is found by letting the total velocity potential $\Phi = \phi + \phi_{\mathrm{I}}$ satisfy Bernoulli's equation,

$$p-p_0=-\rho\frac{\partial\Phi}{\partial t}-\frac{1}{2}\rho|\nabla\Phi|^2-\rho gz \quad (15)$$

where z is the vertical distance from the mean free surface. An expression for the pressure on an element

midpoint can be obtained by rewriting the $\partial\Phi/\partial t$ term using a generalization of the substantial derivative. If the body is fixed, this becomes

$$p - p_0 = -\rho \frac{D'\Phi}{D't} + \rho U_{\mathrm{ms}} \frac{\partial \Phi}{\partial s} - \frac{1}{2}\rho \left(\frac{\partial \Phi}{\partial s} \right)^2 - \rho g z \qquad (16)$$

where D′/D′t yields the change with time when the midpoint of an element is followed, $\partial/\partial s$ is the spatial derivative along the body surface, and U_{ms} is the tangential velocity of the element midpoint. Here, U_{ms} is not the fluid velocity, but the velocity obtained as a consequence of the fact that the midpoints of elements change position. Since the body is fixed, the midpoint has zero normal velocity. Once the pressure distribution on the body is determined, the resulting vertical force on the platform deck can be evaluated by

$$F_3 = -B \int_{S_{\mathrm{B}}} (p - p_0) n_3 \mathrm{d}S \qquad (17)$$

Alternatively, the force on the deck can be found by imposing the conservation of fluid momentum.[11] For the present case, the vertical force can be expressed as

$$\mathbf{F} = \rho B \frac{\mathrm{d}}{\mathrm{d}t} \int_{S_{\mathrm{F}}+S_{\mathrm{B}}} \Phi \mathbf{n} dS + \rho B \int_{S_{\mathrm{F}}+S_{\mathrm{B}}} g z \mathrm{d}S + \rho B \int_{S_\infty} \left(\nabla\Phi \frac{\partial \Phi}{\partial n} - \frac{1}{2} |\nabla\Phi|^2 \mathbf{n} \right) \mathrm{d}S \qquad (18)$$

where S_∞ comprises the vertical control surfaces, and ranges from $z = -\infty$ to $z = 0$ at $|x| = x_b$, and S_{F} is the instantaneous free surface inside $|x| < x_b$.

As a verification of the numerical method, one can compare results for the force acting on the body based on direct pressure integration and conservation of momentum. If the boundary-value problem is solved correctly, these alternative approaches yield the same force on the body. Figure 7 shows a typical comparison. The impact condition in this case is characterized by the wave period $T = 1.43$ s, wave height $H = 0.12$ m, and deck clearance above mean free surface $\eta_{ag} = 0.06$ m. Initially, the alternative force calculations compare very well. This suggests that the integrations of the surface elevation and the velocity potential on the free surface were done correctly. Moreover, it also suggests that the body/free-surface intersection points are well predicted. During the final part of the water impact process, however, the two force estimates diverge. This implies that the solution of the boundary value problem at this stage has become inaccurate.

An important error source is associated with the theoretical modeling of the problem. The total velocity potential is divided into a perturbation velocity potential and the incident velocity potential. This leads to the body boundary condition given in Eq. 10, where $\partial\phi_{\mathrm{I}}/\partial n$ on S_{B} is found by a Taylor expansion about the mean free surface. Strictly speaking, this condition is only valid on the part of the body surface that intersects with the incident wave. By imposing Eq. 10 on the entire wetted body surface, continuity of fluid mass is violated. This leads to nonphysical flows that will affect the force calculations. Even though it is especially severe during the water exit phase in the present problem, this dilemma will also occur for other nonlinear problems when using the body boundary condition in Eq. 10. Figure 8 is a sketch of the wave profile during the final part of the impact process and the undisturbed wave. The exact free surface is very different from the incident wave described by ϕ_{I}. The body boundary condition used may not be accurate enough at this stage of the process.

Extensive convergence studies and comparisons with experiments are presented elsewhere.[9] The convergence tests show that the method converges well when the number of elements on the free surface and on the wetted body surface are increased, and when the time-increment used in the time integration is decreased.

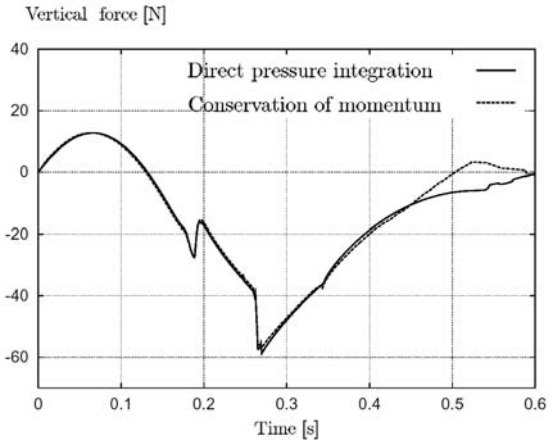

Fig. 7. Comparison of the results from direct-pressure integration and the conservation of fluid momentum when the boundary-value problem is solved for the perturbation velocity potential. $T = 1.43$ s, $H = 0.12$ m, and $\eta_{ag} = 0.06$ m

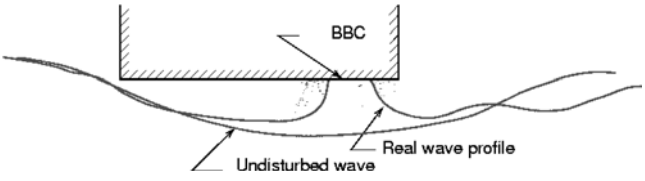

Fig. 8. A sketch of the exact and undisturbed wave profiles during the final stage of water exit

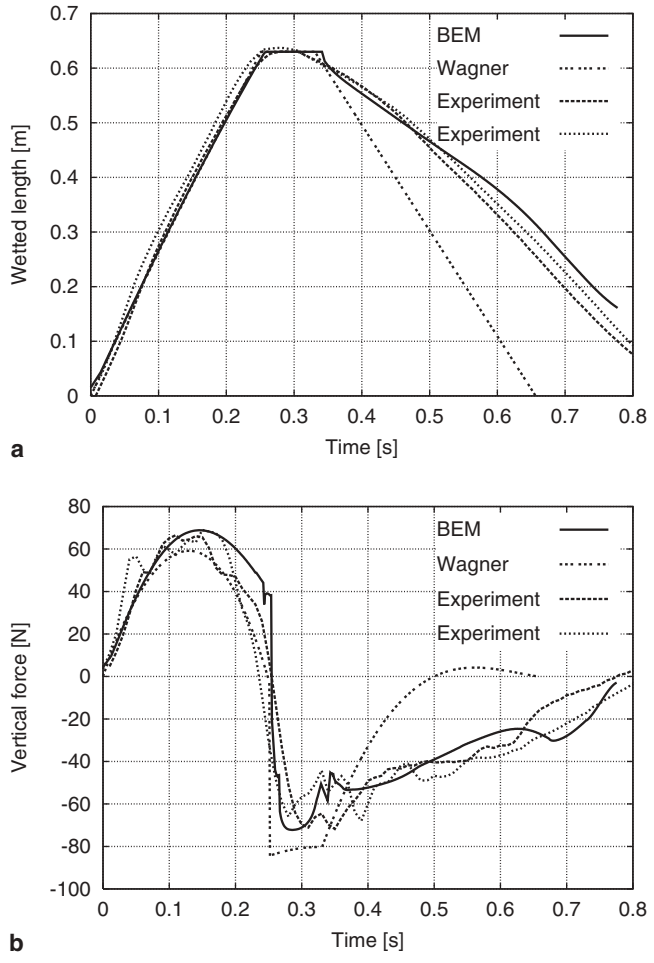

Fig. 9. Comparison between experiments and numerical results from the Wagner-based method and the boundary-element methods for perturbation potential. T = 1.25 s, H = 0.12 m and η_{ag} = 0.04 m

From sensitivity studies, it is concluded that $\phi_F = \pi/10$ is a good value to use. Figure 9 shows a typical comparison between experiments and numerical simulations. Two experimental time-series are shown to indicate the experimental accuracy. The force from the boundary element method (BEM) is found by direct pressure integration. One can see that the Wagner-based method (WBM) provides good predictions for both the magnitude and the duration of the water entry force, while the results for the water exit phase are less satisfactory. In general, the WBM overestimates the magnitude and underestimates the duration of the water exit force. The latter is caused by the von Karman approach being applied to describe water exit. The BEM proves to be a significant improvement. The duration of the water impact process is well predicted for most of the impact cases tested, and the numerical and experimental force histories also compare well for the entire water entry/water exit process. For water exit in particular, the BEM is superior to the WBM, although instabilities occur in the final part of this phase. However, the force on the body is small at this stage. More comparisons are given elsewhere.[8,9]

There are different reasons why the BEM gives better predictions then the WBM during the water exit phase. One is the inclusion of the Kutta condition. Another reason is that the dynamic free-surface condition $\phi = 0$ is valid in a limited initial time-period, and becomes less accurate during the water exit phase. In fact there is an inconsistency in the WBM during the water exit phase. Using the kinematic free-surface condition which is consistent with $\phi = 0$ on the free surface to find the body free-surface intersection during the water exit phase does not give a solution. That is why we have to use a von Karman-type approach during the water exit phase when the WBM is used. The dynamic free-surface condition used in the BEM tells us how ϕ is changing on the free surface. One of the contributions is due to gravity. An obvious way to study the effect of including gravity in the boundary value problem is to solve it with and without gravity included, and to compare the results directly. This was not possible with the present boundary element method. If gravity is turned off, the jet at the upstream side wall does not come back down. Thus, the computer code cannot handle the flow around the front edge without the aid of gravity. Gravity allows wave-making to occur, which is in accordance with observations in the laboratory. When a linear hydrodynamic system is studied, the body's ability to create waves is directly connected to its damping properties. Even if our hydrodynamic system is nonlinear, the study of a related linear hydrodynamic problem can assess the importance of the generation of free-surface waves. The importance of gravity can thus be studied by an evaluation of the damping coefficient.

Figure 10 shows both theoretical and experimental results for the two-dimensional heave-damping coefficient, $B_{33}^{(2D)}$, for a rectangular cylinder of shallow draft. Vugts[15] reported numerical and experimental results for the beam–draft ratio, b/D, equal to 2, 4, and 8. His experimental results agreed well with the numerical results, but only the numerical results are presented in Fig. 10. For the impact problem, $D = 0$, an extrapolation of Vugts' results to zero draft is included in the figure. MacCamy[16] derived theoretical results for the heave-damping for a thin plate. The figure also contains experimental results presented elsewhere.[9] These were found by measuring the heave excitation force on a fixed rectangular cylinder in regular waves of amplitude ζ_a, and the simple relation

$$F_{3,\mathrm{exc}}^{(2D)} = \zeta_a \sqrt{\frac{\rho g^2}{\omega} B_{33}^{(2D)}} \tag{19}$$

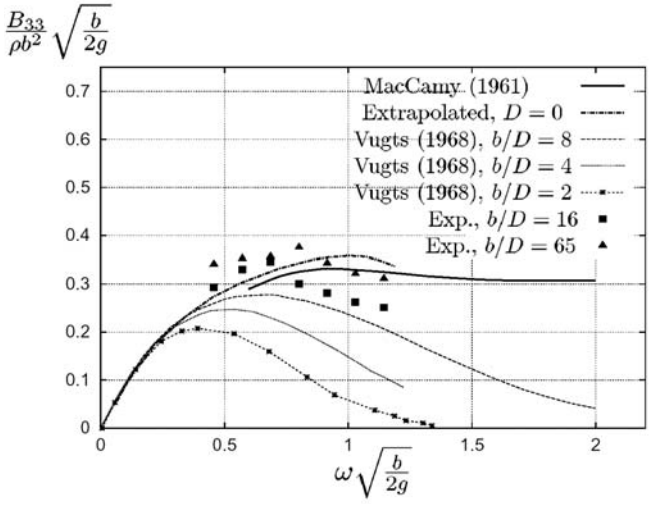

Fig. 10. The two-dimensional damping coefficient $B_{33}^{(2D)}$ in heave for a rectangular cylinder oscillating in a free surface. The figure comprises experimental values for small drafts (from Baarholm[9]), theoretical results by Vugts[15] and MacCamy,[16] and an extrapolation of Vugts' results to zero draft. b and D are cylinder breadth and draft, respectively

derived by Newman[17] gives the damping coefficient, where $F_{3,\mathrm{exc}}^{(2D)}$ is the two-dimensional heave excitation force amplitude. The experiments were performed with $b/D = 16$ and 65, and the results seem reasonable when compared with the theoretical results by Vugts and MacCamy. We applied these results to our impact problem by considering a thin plate with b equal to 0.63 m. The oscillation period T = 1.25 s then gives $\omega\sqrt{b/2g} \approx 0.90$, which means that the damping coefficient that is close the maximum value on the curve for $D = 0$. This implies that considerable wave-making should be expected when the deck used in this study gets fully wetted. However, it should be noted that the previous results are for steady-state conditions, while our case includes the effects of the initial conditions, and a duration less than the period of oscillation, as well as a changing wetted length.

Intuitively, the ratio between the duration of the water impact process and the wave period will affect the significance of gravity. The longer the duration is relative to the period of oscillation, the larger the influence from wave-making will be. For the impact event shown in Fig. 9, this ratio is approximately 0.65. This suggests that gravity is important during the water exit phase. Conversely, Ge[18] found gravity to be of minor importance during water exit for water impact on a wetdeck of a catamaran. This means that a theory neglecting gravity and based on the Wagner/Von Karman method agreed reasonably well with experiments in both the water entry and the water exit phases. In the most severe slamming case in her study $\omega\sqrt{b/2g} \approx 1.14$, and one would expect from Fig. 10 that wave-making should occur, although the ratio between the duration and the wave period was less than 20%.

Boundary-element method for the total velocity potential

As discussed above, solving the problem for the perturbation velocity potential leads to inconsistencies, and the solution during the final part of water exit is not good. Therefore, we attempted to solve the problem for the total velocity potential instead. This method is very similar to the one described above, but a few modifications are required. The boundary value problem is solved as an initial value problem with an initial condition $\Phi = \phi_I$ on $z = \zeta_I$, where ϕ_I and ζ_I denote the velocity potential and the elevation of the incident waves, respectively. The inside of the fluid domain Φ is represented by Green's second identity (with Eq. 11, with ϕ replaced by Φ). The enclosing surface $S = S_B + S_F + S_\infty$, where S_∞ comprises the vertical control surfaces at $x = \pm x_b$. If the control surface is placed sufficiently far from the body, one can assume that the flow is undisturbed, and one can set $\Phi = \phi_I$ and $\partial\Phi/\partial n = \partial\phi_I/\partial n$ on S_∞. Thus, the integration over S_∞ in Eq. 11 is straightforward numerically. As before, Φ is known and $\partial\Phi/\partial n$ in unknown on the free surface, while Φ is unknown and $\partial\Phi/\partial n$ is known on the body surface. The time-integration and the evaluation of the body/free surface intersection points are performed in the same manner as in the former boundary-element method. The Kutta condition is also imposed in the same way as before.

To ensure undisturbed conditions at the far field control surfaces, damping layers are included on the free surface close to these surfaces. Artificial damping (sponge layer) of the parts of the velocity potential and wave elevation that are different from Stokes waves is applied. An artificial dissipative term is added explicitly to the free-surface condition so that the disturbance is absorbed with as little wave reflection as possible. Damping layers are discussed elsewhere.[19] With dissipative terms added, the kinematic and dynamic free-surface conditions can be written as

$$\frac{D\Phi}{Dt} = \frac{1}{2}\left[\left(\frac{\partial\Phi}{\partial x}\right)^2 + \left(\frac{\partial\Phi}{\partial z}\right)^2\right] - g\zeta - \nu(x)\left(\Phi - \phi_I\right) \tag{20}$$

and

$$\frac{\partial\zeta}{\partial t} = \frac{\partial\Phi}{\partial z} - \frac{\partial\Phi}{\partial x}\frac{\partial\zeta}{\partial x} - \nu(x)\left(\zeta - \zeta_I\right) \tag{21}$$

respectively, where the Rayleigh damping terms $\nu(x)$ $(\Phi - \phi_I)$ and $\nu(x)(\zeta - \zeta_I)$ are specified to be nonzero in

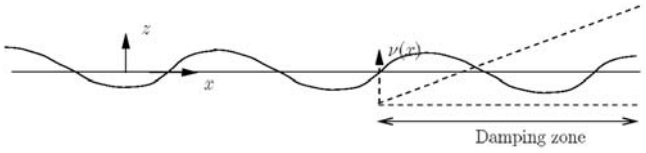

Fig. 11. Damping layer with linearly increasing artificial viscosity coefficient $\nu(x)$

the damping zone and zero elsewhere, $\nu(x)$ is taken to be a linear function that increases from zero at the beginning of the damping zone to a given positive value at the end of the zone (Fig. 11), and ν has dimension frequency, and its maximum value in this work is given by $\nu_{\max} = C_\nu \sqrt{g/\lambda}$ (where $C_\nu = 0.5$ and λ is the wave length). The length of the damping layer is set to be equal to the wavelength. The results do not seem to be very sensitive to the damping layer.

To obtain accurate results, the discretization of the problem must be chosen carefully. It is important that the density of the elements is high in regions where the spatial variation of the field variables is high. In the present problem, this is especially the case on the free surface in the vicinity of the body, and on the wetted body surface itself. On the body, a high density of elements is necessary close to its intersections with the free surface. "Far" away from the body, the density of free-surface elements can be lower than close to the body, but a relatively high number of elements is still needed per wavelength to propagate the wave accurately. Farther than half a wavelength away from the body, a constant element size is used in the computer program. Small elements on the control surfaces are chosen near the free surface where the velocity potential and the fluid velocities vary greatly with the vertical coordinate. Farther down in the fluid, longer elements can be used.

In the two former methods, second-order theory was used to describe the incident waves. In reality, wave impact may occur for very steep waves, and second-order theory may not be sufficient to obtain reliable estimates of the wave kinematics in the crest. A higher-order theory is therefore desirable. For deep-water (Stokes) waves for which the dispersion and the nonlinear modification are in balance, analytical solutions in the form of perturbation expansions exist for two-dimensional water waves of permanent shape. The fifth-order Stokes wave is much used for engineering purposes. A number of computer-based methods have been developed to extend the wave to even higher orders by using numerical schemes. A review of such methods is given elsewhere.[20] In this work, the method proposed by Bryant[21] is used to describe the "exact" profile and velocity potential of the undisturbed waves. Bryant represents deep-water Stokes waves by truncated Fourier series for ϕ_I and ζ_I. On dimensionless form, the Fourier series looks like

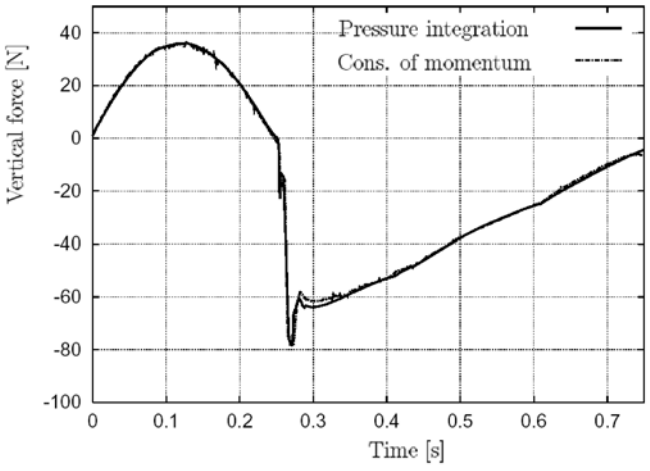

Fig. 12. Comparison between direct-pressure integration and conservation of momentum when solving the boundary-value problem for the total potential. $T = 1.25$ s, $H = 0.10$ m, and $\eta_{ag} = 0.04$ m

$$\bar{\zeta}_I = \sum_{k=1}^{N} a_k \cos\left(k\left(\bar{x} - c\bar{t}\right)\right) \tag{22}$$

and

$$\bar{\phi}_I = \sum_{k=1}^{N} b_k e^{k\bar{z}} \cos\left(k\left(\bar{x} - c\bar{t}\right)\right) \tag{23}$$

where $(\bar{x},\ \bar{z},\ \bar{\zeta}_I) = 2\pi(x,\ z,\ \zeta)/\lambda$, $\bar{t} = t\sqrt{2\pi g/\lambda}$, and $\bar{\phi}_I = \phi_I\, 2/H\sqrt{2\pi/\lambda}$. The number of harmonics used is determined by trial and error, so that the set of Fourier coefficients includes all the amplitudes greater than some prescribed value. When all the coefficients in Eqs. 22 and 23 are known, deriving similar expressions for the water particle velocities and accelerations, and the dynamic pressure in the fluid is straightforward. A major advantage when using this approach compared to the second-order Stokes theory is that one does not have to use a Taylor expansion to get estimates for values of physical quantities above the mean free surface. Equation 23 is valid all the way up to $\bar{z} = \bar{\zeta}$. For the cases studied in this work, the error made by using second-order theory for the incident wave compared with the more exact formulation is insignificant. Figure 12 shows a typical comparison for the vertical force on the deck computed by direct pressure integration and by conservation of momentum. The wave period and height are 1.25 s and 0.10 m, respectively, while the deck clearance in calm water is 0.04 m. Good agreement between the two alternative methods can be seen for the entire impact process. Figure 13 shows comparisons

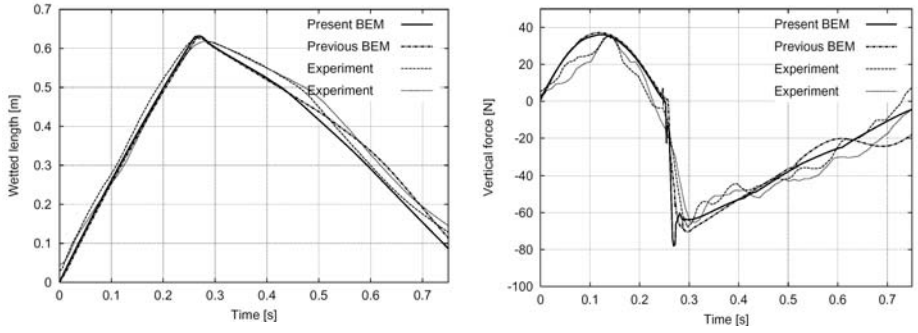

Fig. 13. Comparisons between experiments and boundary-element methods that solve the boundary value problem for perturbation potential (previous) and for total velocity potential (present). $T = 1.25\,\mathrm{s}$, $H = 0.10\,\mathrm{m}$, and $\eta_{ag} = 0.04\,\mathrm{m}$

between theory and experiments for the wetted length and the vertical force for the same impact conditions. The theoretical forces are evaluated by direct-pressure integration. The method presented here gives results that are in excellent agreement with experiments.

Conclusions

Water impact on a platform deck may be divided into the water entry phase and the water exit phase. A positive slamming force dominates the former phase, while a negative added mass force dominates the latter. Except from the most violent impact events studied in the experiments, the magnitude of the negative force peak is greater than that of the positive force peak for two-dimensional flow conditions. Thus, the water exit phase is important for global effects. However, the largest averaged pressures occur during the initial water entry phase, which is the most important for local structural effects.

Three numerical methods have been used to assess the vertical impact force on the deck due to regular incident waves. Theoretical results have been compared with experimental results. The Wagner-based method which neglects gravity yields satisfactory results for water entry, but poor results for both the magnitude of the force and the duration of the water exit phase. A von Karman approach was used during water exit. The boundary-elements methods provide good results for the time-history of the wetting of the deck and the vertical impact force for the entire impact process. For the water exit phase in particular, they offer important improvements over the Wagner-based method. The Kutta condition imposed at the aft end of the deck is crucial in order to get good results, and it is shown that by also using this condition in the final part of the exit phase, when the downstream intersection point propagates upstream, it is possible to obtain stable results almost until the deck is dry. The method in which the total velocity potential is solved is more consistent, and better results are obtained for the final part of water exit. In this phase, however, the load on the deck is small.

An obvious weakness of the present methods is that they all assume two-dimensional flow. In reality, three-dimensional effects are important, and one should consider extending the method to three dimensions. In principle, this is straightforward, but one needs to reflect carefully on how to impose the Kutta condition in a three-dimensional model.

References

1. Dalton C, Nash JM (1976) Wave slam on horizontal members of an offshore platform. In: Proc of the 8th Offshore Technology Conference. Offshore Technology Conference, Houston, pp 749–758
2. Faltinsen OM, Kjærland O, Nøttveit A (1977) Wave impact loads and dynamic response of horizontal cylinders in offshore structures. In: Proc of the 9th Offshore Technology Conference. Offshore Technology Conference, Houston, pp 119–126
3. Sarpkaya T (1978) Wave impact loads on cylinders. In: Proc of the 10th Offshore Technology Conference. Offshore Technology Conference, Houston, pp 169–176
4. Broughton P, Horn E (1987) Ekofisk platform 2/4C: re-analysis due to subsidence. Proc Inst Civ Eng Part 1: 949–979
5. Wagner H (1932) Uber Stoss- und Gleitvorgange an der Oberflache von Flussigkeiten. ZAMM 12:192–214
6. Baarholm R, Faltinsen OM (2000) Experimental and theoretical studies of wave impact on an idealized platform deck. In: Proc of the 4th Int Conf on Hydrodynamics (ICDH 2000). ICHD 2000 Local Organizing Committee, Yokohama
7. Baarholm R, Faltinsen OM, Herfjord K (2001) Water impact on decks of floating platforms. In: Proc of the 8th Int Symp on Practical Design of Ships and other Floating Structures (PRADS2001). Elsevier, Oxford
8. Baarholm R, Faltinsen OM (2001) A boundary-element method for solving water impact on a platform deck. In: Proc the 20th Offshore and Arctic Engineering Conference (OMAE 2002). ASME, New York
9. Baarholm R (2001) Theoretical and experimental studies of wave impact underneath decks of offshore platforms. PhD Thesis, Norwegian University of Science and Technology, Trondheim
10. Kaplan P (1992) Wave impact on offshore structures: re-examination and new interpretations. In: Proc of the 24th Offshore Technology Conference. Offshore Technology Conference, Houston, pp 79–86
11. Faltinsen OM (1977) Numerical solutions of transient nonlinear free-surface motions outside or inside moving bodies. In: Proc of

the 2nd Int Conference of Numerical Ship Hydrodynamics, University Extension Publications, University of California, Berkeley
12. Zhao R, Faltinsen OM (1993) Water entry of two-dimensional bodies. J Fluid Mech 246:593–612
13. Faltinsen OM, Greco M, Landrini M (2003) Green water and slamming on a VLFS with shallow draft. 4th Int Workshop on Very Large Floating Structures, Tokyo
14. Faltinsen OM, Pettersen B (1987) Application of a vortex tracking method to separated flow around marine structures. J Fluid Struct 1:217–237
15. Vugts JH (1968) The hydrodynamic coefficients for a swaying, heaving and rolling cylinder on a free surface. Technical Report 112 S, Netherlands Ship Research Centre TNO, Technological University Delft
16. MacCamy RC (1961) On the heaving motion of a cylinder of shallow draft. J Ship Res 5(4):34–42
17. Newman JN (1962) Exciting forces on fixed bodies in waves. J Ship Res 6(4):10–17
18. Ge C (2002) Global hydroelastic response of catamarans due to wetdeck slamming. PhD Thesis, Norwegian University of Science and Technology, Trondheim
19. Israeli M, Orszag SA (1981) Approximation of radiation boundary conditions. J Comp Phys 41:115–135
20. Schwartz LW, Fenton JD (1982) Strongly nonlinear waves. Annu Rev Fluid Mech 14:39–60
21. Bryant JP (1983) Waves and wave groups in deep water. In: Debnath L (ed) Nonlinear waves. Cambridge University Press, Cambridge